PLATELETS AND THROMBOPOIESIS

Myosin IIA is critical for organelle distribution and F-actin organization in megakaryocytes and platelets

Fabien Pertuy, Anita Eckly, Josiane Weber, Fabienne Proamer, Jean-Yves Rinckel, François Lanza, Christian Gachet, and Catherine Léon

Unité Mixte de Recherche S949, Institut National de la Santé et de la Recherche Médicale–Université de Strasbourg, Etablissement Français du Sang–Alsace, Strasbourg, France

Key Points

- Myosin IIA deficiency affects F-actin structuration and organelle distribution in MKs which leads to abnormal platelet organelle content.

During proplatelet formation, a relatively homogeneous content of organelles is transported from the megakaryocyte (MK) to the nascent platelets along microtubule tracks. We found that platelets from *Myh9*$^{-/-}$ mice and a MYH9-RD patient were heterogeneous in their organelle content (granules and mitochondria). In addition, *Myh9*$^{-/-}$ MKs have an abnormal cytoplasmic clustering of organelles, suggesting that the platelet defect originates in the MKs. Myosin is not involved in the latest stage of organelle traffic along microtubular tracks in the proplatelet shafts as shown by confocal observations of proplatelet buds. By contrast, it is required for the earlier distribution of organelles within the large MK preplatelet fragments shed into the sinusoid circulation before terminal proplatelet remodeling. We show here that F-actin is abnormally clustered in the cytoplasm of *Myh9*$^{-/-}$ MKs and actin polymerization is impaired in platelets. Myosin IIA is required for normal granule motility and positioning within MKs, mechanisms that may be dependent on organelle traveling and tethering onto F-actin cytoskeleton tracks. Altogether, our results indicate that the distribution of organelles within platelets critically depends on a homogeneous organelle distribution within MKs and preplatelet fragments, which requires myosin IIA. (*Blood*. 2014;123(8):1261-1269)

Introduction

Platelets play a pivotal role in hemostasis and in several other aspects of vascular biology such as atherosclerosis, angiogenesis, or wound healing, partly through secretion of their granule contents. α and dense granules, the 2 functionally most important secretory granules in platelets, store numerous platelet-activating factors as well as coagulation, angiogenic, and mitogenic factors. Platelets are produced by megakaryocytes (MKs) through a well-regulated process of differentiation and maturation. Granule biogenesis begins between stages I and II of MK differentiation[1] and involves both biosynthetic and endocytic pathways.[2] In the final steps of maturation, MKs shed cytoplasmic processes into the sinusoid vessels of the marrow.[3] On the basis of in vitro observations, these processes called proplatelets have been described as thin and highly branched,[4] with the tip of a proplatelet forming the proplatelet bud, whose size corresponds to the future platelet.

During proplatelet formation, constant and homogeneous amounts of components and organelles of the future platelet need to be distributed into the proplatelet bud, which is defined as the nascent platelet. A previous in vitro study showed that organelles are not transported as preformed "platelet units" but individually from the MK into the maturing platelet bud.[5] Microtubules play an essential role in this transport by forming tracks along which kinesin-linked granules and mitochondria traffic. Organelles are eventually trapped once they enter the proplatelet tip, where they continue to circle along the microtubule coil.[5] During final platelet maturation, the organelles detach from the microtubule coil to adopt an apparently random subcellular location within the platelet. The mechanisms controlling the transport of granules/organelles from the MK cytoplasm into proplatelets and allowing the organelles to detach from the microtubule coil are still unknown, as is the way in which a relatively constant number of organelles is packaged within each platelet.

In the present report, we show that myosin IIA plays a critical role in the distribution of organelles within platelets and bone marrow MKs. We show here that myosin deficiency leads to defective actin cytoskeleton structuration which may impair granule distribution during MK maturation. Our data reveal that myosin is not involved in the latest stage of organelle transport along microtubular tracks in the proplatelet shafts. By contrast, it turns out that it is necessary for the earlier distribution of organelles within MKs and hence within the large MK fragments shed into the sinusoid circulation, before terminal proplatelet remodeling and platelet shedding.

Materials and methods

Materials

Materials are described in supplemental Methods (available on the *Blood* Web site).

Submitted June 12, 2013; accepted November 12, 2013. Prepublished online as *Blood* First Edition paper, November 15, 2013; DOI 10.1182/blood-2013-06-508168.

The online version of this article contains a data supplement.

The publication costs of this article were defrayed in part by page charge payment. Therefore, and solely to indicate this fact, this article is hereby marked "advertisement" in accordance with 18 USC section 1734.

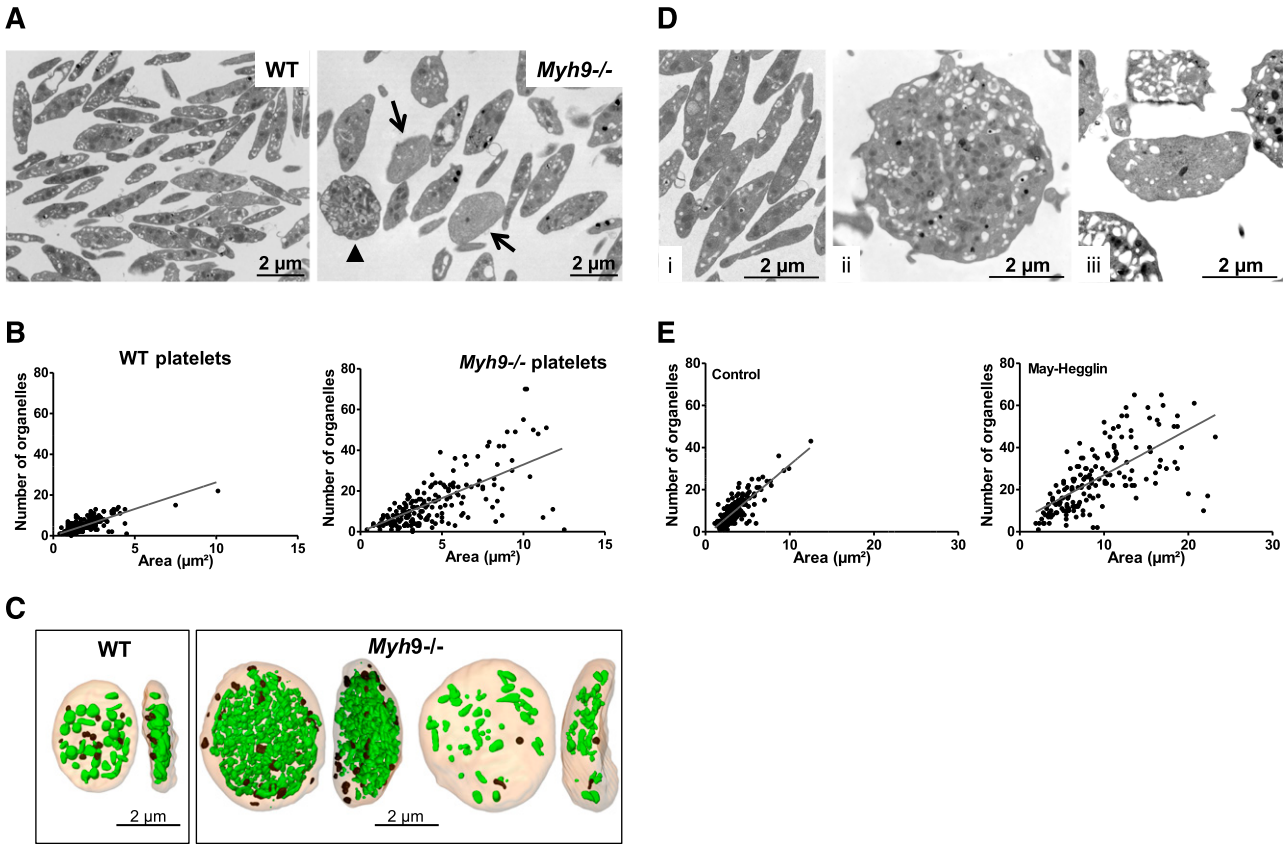

Figure 1. Abnormal distribution of organelles in mouse *Myh9*$^{-/-}$ and human MYH9-RD platelets. (A) Wide-field electron micrographs of mouse platelets showing the heterogeneous content of *Myh9*$^{-/-}$ platelets (right) as compared with WT cells (left). Arrows point to low-content platelets and the arrowhead to a high-content platelet. (B) Quantification of the total number of organelles (α and δ granules, lysosomes, and mitochondria) per platelet as observed by TEM. The number of organelles is plotted as a function of the platelet size, and 215 and 190 platelets were analyzed for WT and *Myh9*$^{-/-}$ mice, respectively. $P < .0001$ for comparison of variances in the point distribution between WT and *Myh9*$^{-/-}$ mice. (C) 3D reconstructions from an FIB/SEM analysis showing the face and profile views of 1 WT (left) and 2 *Myh9*$^{-/-}$ platelets (right). Note the strong heterogeneity in the organelle contents of the *Myh9*$^{-/-}$ platelets as compared with the WT one. (D) Ultrastructure of human platelets from a control individual (i) as compared with a MYH9-RD patient (ii-iii). (E) Quantification of the number of organelles (α and δ granules, lysosomes, and mitochondria) per platelet as a function of the platelet size, for the MYH9-RD patient (right) and a normal donor (left). Organelles were counted in 178 and 170 platelets for the control and patient, respectively. $P < .0001$ for comparison of variances in the point distribution.

Mice

The floxed *Myh9* strain was crossed with PF4-Cre mice as described previously[6] to obtain animals with deletion of exon 1 of the *Myh9* gene (*Myh9*$^{-/-}$ mice) in the megakaryocytic lineage. All mice in this study had a C57BL/6J genetic background. Animals were used in accordance with the European laws and the Etablissement Français du Sang (EFS) Review Board regarding animal care.

Patient

Patient S.D., aged 55 years at the time of the study, presented an already reported *MYH9* (p.Asp1424Asn) mutation[7] (see supplemental Methods). The patient provided written informed consent in accordance with the Declaration of Helsinki.

Washed platelet preparation and organelle isolation and immunolabeling

Human or mouse blood was centrifuged to obtain platelet-rich plasma, and platelets were washed in Tyrode-albumin buffer as previously described.[8] For organelle isolation, human platelets (1-2 × 10^9 in 13 mL) were disrupted by nitrogen cavitation and organelles isolated on Percoll gradient (see supplemental Methods).

Electron microscopy

For transmission electron microscopy (TEM), pellets of washed platelets or flushed bone marrow cells were fixed in 2.5% glutaraldehyde and embedded in Epon as described.[9] For immunolabeling, platelets or organelles were fixed in 2% paraformaldehyde and 0.2% glutaraldehyde, infiltrated with 2.3M sucrose, and frozen in liquid nitrogen.[9] Focused ion beam (FIB)/scanning electron microscopy (SEM) was used to visualize the entire platelet at the resolution of electron microscopy. Three-dimensional (3D) reconstructions were obtained with Amira software (version 5.4; Visualization Sciences Group). See supplemental Methods for details on all the EM procedures.

In vitro MK differentiation and proplatelet formation

Mouse MKs were differentiated in vitro as previously described[10] (see supplemental Methods for details).

F-actin visualization

For visualization of F-actin in bone marrow MKs, mouse femurs were directly flushed into 4% formaldehyde containing 4 × 10^{-5}M taxol and labeled (see supplemental Methods).

Videomicroscopy and organelle tracking

Megakaryocytes cultured for 5 days were incubated for 2 hours with AF-488–fibrinogen (150 μg/mL) as described,[5] washed, and allowed to adhere on poly-L-lysine for 2 hours (see supplemental Methods). Fluorescence was recorded for 5 minutes and organelle tracking performed using Imaris software (version 7.5). Data correspond to 9 to 10 videos for each genotype acquired from 3 independent experiments, resulting in 5260 tracks for wild-type (WT) organelles and 3479 tracks for *Myh9*$^{-/-}$ organelles.

Statistical analyses

The dispersion of organelle contents in platelets and platelet buds was analyzed with R software (version 2.15.2). The residuals of the samples, calculated as the distance between each point and the regression line, were tested for normality using the Shapiro test ($n > 30$). For each comparison between *Myh9*$^{-/-}$ or MYH9-RD cells and controls, the variance of the residuals was tested using the Levene test with an α risk of 5% and a 1-sided *P* value.

Statistical analyses of organelles mean speed and displacement were performed using the Mann-Whitney nonparametric test with an α risk of 5% and a 2-sided *P* value.

Results

Deletion or mutation of the myosin IIA gene leads to an abnormal platelet organelle distribution

Myh9$^{-/-}$ platelets are heterogeneous in size, with an increased mean platelet volume (6.28 ± 0.08 fL compared with 4.84 ± 0.03 fL for WT platelets, n = 12 mice, $P < .0001$), and they contain larger amounts of rough endoplasmic reticulum (RER) as previously described.[6] Myosin deficiency also led to an abnormal distribution of organelles (α and δ granules and mitochondria) within platelets. Using TEM, we found that some platelets had a gray appearance, containing few organelles and an open canalicular system (OCS), while others were crowded with organelles (Figure 1A). Platelets displaying a gray appearance, with <5 organelles per TEM section were quantified and qualified as "low-content" platelets. These represented 22.3% ± 2.2% in *Myh9*$^{-/-}$ mice vs 4% ± 1.3% in WT mice (mean ± standard error of the mean [SEM], n = 297-301 platelets from 3 mice) (arrows, Figure 1A). These observations suggested an abnormal organelle distribution in *Myh9*$^{-/-}$ platelets. A quantitative representation of the organelle content of WT and *Myh9*$^{-/-}$ platelets according to the platelet size (Figure 1B) illustrates this heterogeneity ($P < .0001$, comparing the variance of the distributions in WT and *Myh9*$^{-/-}$ platelets).

To visualize the spatial organelle distribution within platelets, we examined whole platelets using "dual beam" electron microscopy (FIB/SEM). This technique allows the observation of large-volume samples by acquisition of serial sections of 20 nm thickness. Although it was not possible to precisely quantify the number of platelets, we observed the presence of "low-content" and "high-content" platelets in *Myh9*$^{-/-}$ image stacks (supplemental Videos 1-2, see arrows and arrowheads). Some of these platelets were entirely analyzed by manual segmentation delineating every organelle in each platelet section, which meant analyzing up to 220 sections, depending on the cell size and orientation. Subsequently, 3D images were reconstructed to visualize the entire platelet and its organelle content. Figure 1C and supplemental Videos 3-5 show the 3D reconstructions of a low-content and a high-content platelet, as compared with a WT platelet. The WT platelet contains 33 organelles (granules, lysosomes, and mitochondria) including 12 dense granules recognized by their typical dense aspect, for a volume of 4.6 μm^3 (organelle:volume ratio of 7.2). The high-content *Myh9*$^{-/-}$ platelet contains 341 organelles including 37 dense granules in a volume 4.3 times larger than the WT volume (19.7 μm^3) (organelle:volume ratio of 17.3), whereas the low-content platelet contains 48 organelles (2 dense granules) in a volume 3.3 times larger than the WT volume (15.47 μm^3) (organelle:volume ratio of 3.1) (Figure 1C).

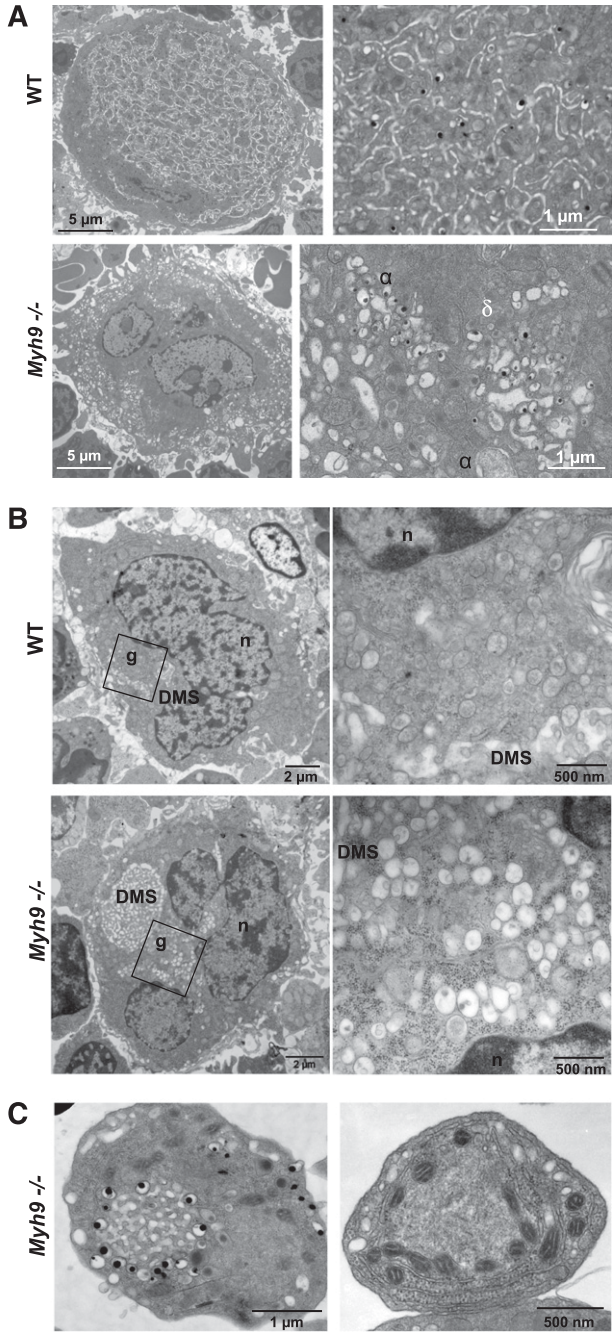

Figure 2. Abnormal MK distribution upon maturation of *Myh9*$^{-/-}$ MKs. (A) TEM images showing the in situ ultrastructure of WT (top panels) and *Myh9*$^{-/-}$ (bottom panels) MKs. Higher magnifications (right images) show the normal granule distribution in the WT cytoplasm and clusters of α (α) and dense (δ) granules in *Myh9*$^{-/-}$ MKs. (B) TEM observations of in situ bone marrow showing the presence of granule clusters (g) located near the nucleus (n) and the developing pre-DMS in immature stage I WT (top panels) and *Myh9*$^{-/-}$ (bottom panels) MKs. Right images are magnification of left images. (C) Detail showing the abnormal organelle positioning in platelets from *Myh9*$^{-/-}$ mice. (Left) Dense granules aligned around membrane complex. (Right) Mitochondria aligned along the RER.

To determine whether the mutations in MYH9-RD patients lead to similar defects, we analyzed platelets from a patient with an *MYH9* p.Asp1424Asn mutation. This patient exhibited giant platelets having a heterogeneous distribution of the platelet granules and mitochondria, very similar to the phenotype observed in the mouse model (Figure 1D-E). Overall, these results demonstrate a role of myosin IIA in the distribution of organelles in platelets.

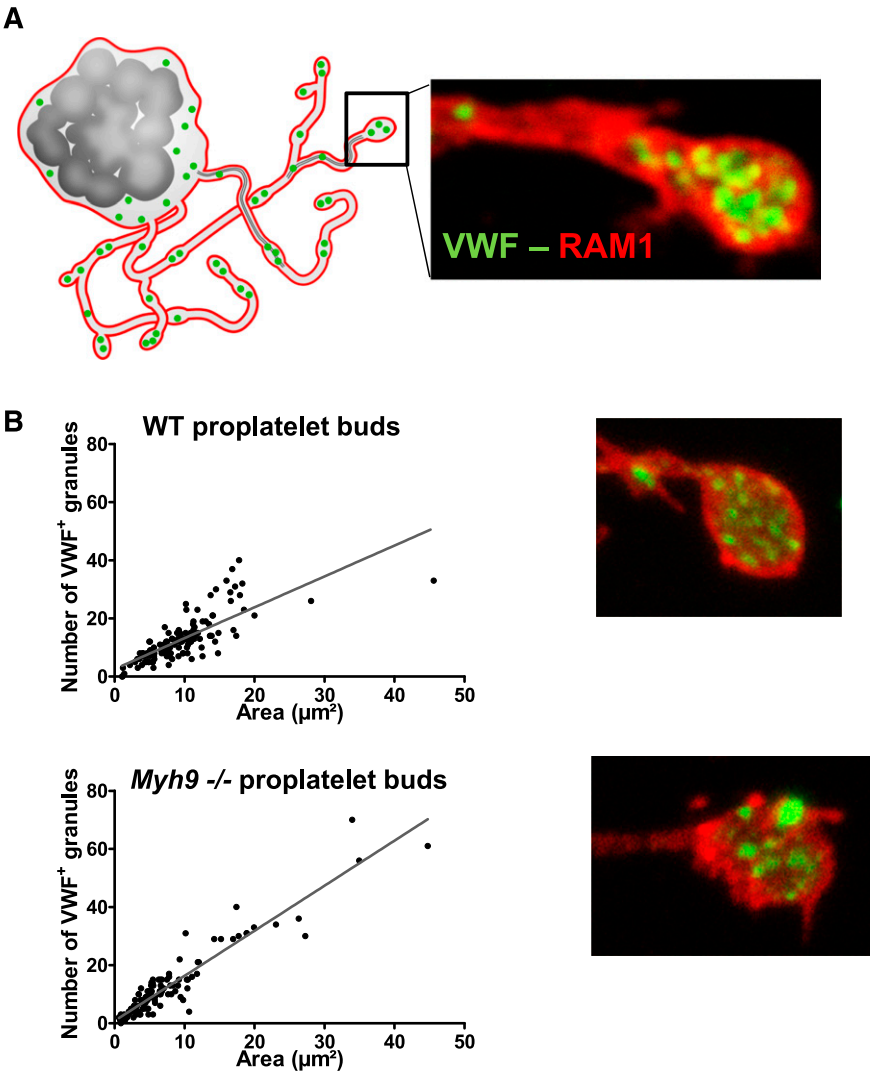

Figure 3. Granule distribution in proplatelet buds. (A) Cultured MKs bearing proplatelets were imaged after immunolabeling with anti-GPIbβ (red, RAM1) and anti-VWF antibodies (green). (B) Quantification of the number of VWF-positive granules (green labeling) per proplatelet bud as a function of the bud size. n = 123 proplatelet buds for WT cells, n = 115 proplatelet buds for *Myh9*$^{-/-}$ cells, in 3 separate cultures. The variances in the point distribution were not statistically different.

Myh9$^{-/-}$ MKs have an abnormal cytoplasmic organelle distribution

To elucidate the origin of this heterogeneous platelet content, we looked at how the organelles were distributed within MKs. Bone marrow MKs were examined in situ by TEM. In more mature stage III WT MKs, the granules were evenly distributed within the so-called platelet territories, delineated by the demarcation membrane system (DMS) (Figure 2A). In contrast, *Myh9*$^{-/-}$ bone marrow MKs displayed an abnormal organelle distribution pattern. α and dense granules and mitochondria were frequently observed in clusters, sometimes with organelles of the same type tightly packed (Figure 2A) or with surrounding membrane complexes. Strikingly, similar organelle clusters can be observed in less mature stage I to II WT and *Myh9*$^{-/-}$ MKs, in close proximity to the developing pre-DMS which at this stage appears as a focal membrane complex located near the nucleus[11] (Figure 2B). Overall, these observations suggest that (1) the defect in *Myh9*$^{-/-}$ platelets originates in the precursor cells, before the final maturation stage and prior to granule transport along the proplatelet shafts, and (2) it could result from a defective *Myh9*$^{-/-}$ cytoplasmic maturation.

It is worthy of note that some circulating *Myh9*$^{-/-}$ platelets also contained abnormally clustered organelles reminiscent of the abnormal clustering in MKs. Dense granules could be seen surrounding membranous structures resembling the OCS (Figure 2C, left). In other unusual platelet morphologies, mitochondria or α granules were found positioned in a string-like fashion along the RER, often associated with microtubules (Figure 2C, right). Such organizations are occasionally observed in immature WT MKs (supplemental Figure 1), which again favors the hypothesis of an incomplete maturation process in *Myh9*$^{-/-}$ MKs.

Myosin IIA is not involved in granule transport to proplatelet buds

During proplatelet formation, organelles have been shown to traffic from the MK to the proplatelet buds by moving along microtubular tracks in the proplatelet shafts.[5] To determine whether myosin deficiency affects organelle transport to the proplatelet buds, WT and *Myh9*$^{-/-}$ MKs bearing proplatelets were differentiated in vitro from Lin^{-} cells and analyzed by confocal microscopy after labeling with antibodies against von Willebrand factor (VWF), a specific marker of α granules (Figure 3A). As previously shown,[9] *Myh9*$^{-/-}$ proplatelet buds were larger than WT ones. However, the distribution of VWF-positive granules was similar in WT and *Myh9*$^{-/-}$ MKs, being linear with the bud size (Figure 3B). These results suggested that myosin does not play a major role in granule transport along proplatelet shafts to the proplatelet buds, which was surprising in view of the abnormal granule distribution in *Myh9*$^{-/-}$ platelets. We thus wondered how an

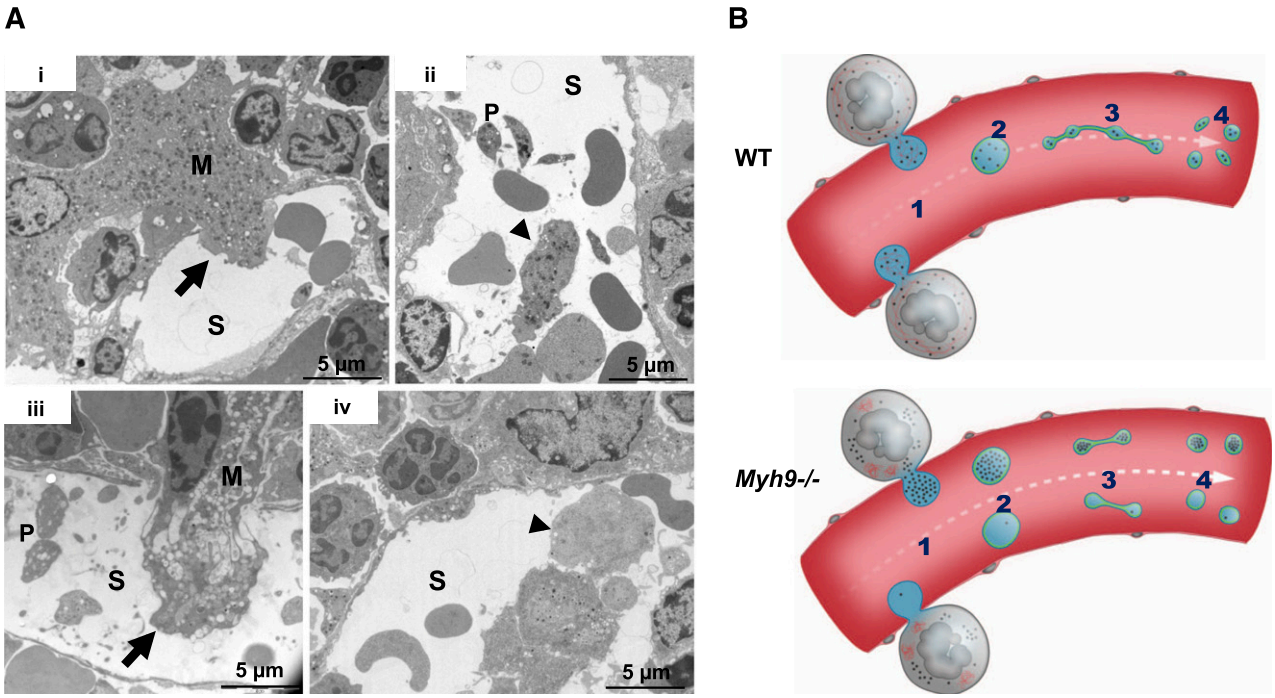

Figure 4. Abnormal distribution of organelles in *Myh9*$^{-/-}$ MK fragments shed into the sinusoids. (A) In situ bone marrow TEM images showing MKs in the process of shedding large fragments into a sinusoid (i,iii) (arrows) or fragments already released (ii,iv) (arrowheads). (i-ii) WT bone marrow; (iii-iv) *Myh9*$^{-/-}$ bone marrow. Note the fragment almost devoid of granules in *Myh9*$^{-/-}$ marrow (iv, arrowhead). S, sinusoid vessel; P, platelet. (B) Scheme recapitulating the importance of organelle positioning within MKs for normal organelle distribution within platelets. An impaired granule distribution in *Myh9*$^{-/-}$ MKs (1) leads to low-content or high-content preplatelet fragments (2) which are reorganized into low-content or high-content platelets (4), despite normal traffic along proplatelets microtubular tracks (3).

organelle distribution defect in MKs could translate into a similar distribution defect in platelets without affecting organelle transport to the proplatelets.

Myh9$^{-/-}$ large MK fragments shed into the sinusoids have an unbalanced granule distribution

To find answers to this apparent paradox, we examined the bone marrow more closely. In native WT bone marrow, we observed some MK fragments in the process of passing through the sinusoids as well as detached large fragments within the sinusoid vessels (Figure 4Ai-ii), in agreement with intravital studies.[12,13] These fragments, larger in size than individual platelets, contained all the organelles that would ultimately be found in the future-released platelets. In *Myh9*$^{-/-}$ bone marrow, the MK fragments were heterogeneous with respect to their organelle distribution and some of them contained very few organelles (Figure 4Aiii-iv). It would seem unlikely that such MK fragments poor in organelles would subsequently be able to remodel into platelets with normal granule content. On the basis of these observations, we propose that the defective granule distribution observed in *Myh9*$^{-/-}$ MKs, which leads to an abnormal granule content in a subset of circulating MK fragments, is responsible for the heterogeneous granule distribution in circulating *Myh9*$^{-/-}$ platelets, despite normal traffic along microtubules in the proplatelet shafts (Figure 4B).

Myosin IIA interacts with the surface of platelet organelles

To understand how myosin may control organelle distribution within MKs, we examined whether myosin IIA was present at the surface of platelet organelles. Human platelet organelles were isolated and washed to eliminate the cytoplasmic myosin pool, and colabeled for myosin IIA and VWF as an α granule marker. Colocalization was observed (Figure 5A), showing that myosin IIA can associate with granules. To achieve a better resolution, immunogold labeling was performed on whole WT mouse platelets and the distribution of myosin according to its intracellular location was quantified by electron microscopy. As expected, myosin was mainly present in the cytosol but also appeared to specifically associate with the cytoplasmic face of organelle membranes (Figure 5B-C). As it has been reported that platelet granules are surrounded with short actin filaments,[14] we investigated whether myosin might interact with organelles through binding to actin. Latrunculin A was used to depolymerize actin filaments in resting human platelets[15] (supplemental Figure 1A). Immunoelectron microscopy analysis showed that incubation of human platelets with latrunculin A (100 μM) for 1 hour did not decrease the myosin IIA labeling at the surface of organelles but rather increased it, possibly through release of myosin from the actin cytoskeleton or unmasking antigens (Figure 5D; supplemental Figure 1B). This suggested that myosin IIA interacts with organelle membranes independently of F-actin. To confirm that this association was specific to organelles, we isolated platelet granules and mitochondria from latrunculin A–treated platelets and performed western blotting experiments on the lysates of these organelles. As expected, latrunculin A treatment decreased the association of F-actin with organelles, but not the association of myosin which appears to be independent on F-actin (Figure 5E). Overall, myosin IIA binds to the surface of platelet organelles, raising the question of a role for this molecular motor in organelle motility.

Absence of myosin IIA affects granule movement

To examine whether organelle movements were affected by absence of myosin IIA, we performed real-time videomicroscopy on living MKs. After 5 days in culture, MKs were incubated with AF-488–fibrinogen to label α granules. In WT cells, fluorescently labeled granules moved in an apparently random manner. Within

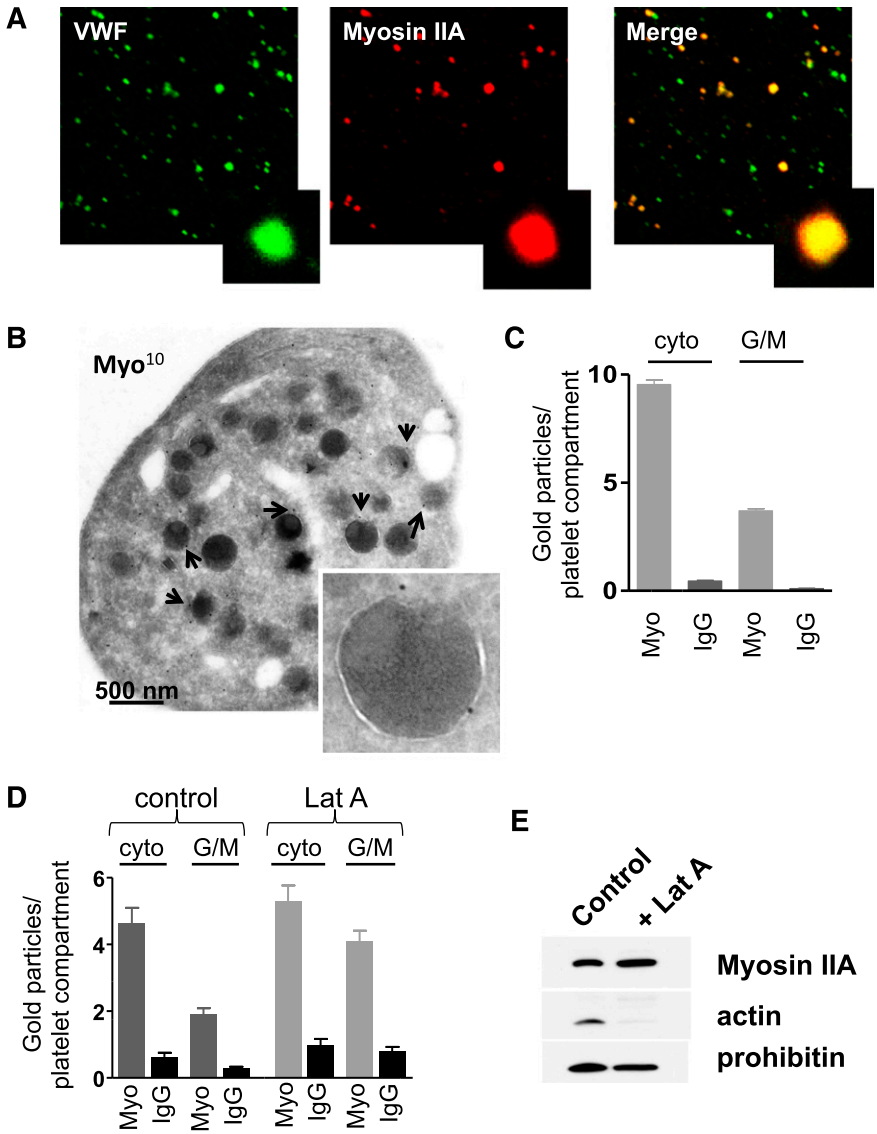

Figure 5. Presence of myosin IIA at the surface of platelet organelles. (A) Confocal observation of isolated human platelet organelles immunolabeled with anti-VWF antibody and anti-myosin IIA antibody showing the presence of myosin at the surface of VWF-positive α granules. (B) Immunogold labeling (anti-myosin IIA, 10 nm) of WT mouse platelets, showing the presence of myosin IIA at the cytoplasmic face of organelles. Inset, α granule labeled with 2 gold particles. (C) Quantification of the numbers of gold particles according to their localization in WT mouse platelets, either cytoplasmic or at the cytoplasmic face of granules or mitochondria. Results are mean ± SEM; n = 20-22 platelets. (D) Quantification of gold particles in human platelets treated or not with latrunculin A (100 μM). Data are mean ± SEM; n = 20. (E) Western blots performed on granules isolated from human platelets pretreated or not with latrunculin A (100 μM). While latrunculin A treatment removed F-actin from the surface of organelles, myosin IIA remained associated with organelles. Prohibitin, a mitochondrial protein, was used as a loading control and blots are representative of 3 separate experiments. cyto, cytoplasmic; G/M, granules or mitochondria; IgG, immunoglobulin G (isotype-matched control antibody); Lat A, latrunculin A; Myo, anti-myosin IIA antibody.

a cell, some granules moved quite fast, with saltatory motion, sometimes with back and forth movements (supplemental Video 6). Others were more stationary, with movements appearing to be confined to a smaller area. In the absence of myosin IIA, some cells clearly exhibited clusters of fluorescently labeled granules (Figure 6A). Although a few granules still had a fast and long distance movement, especially at the periphery of the cell, many of them moved over shorter distances than WT ones (supplemental Video 7). To quantify granule movements, fluorescent granules were tracked in 4 dimensions. In WT MKs, granules moved at a mean speed of 4.63 ± 0.04 μm × min^{-1} (mean ± SEM) that was similar to *Myh9*$^{-/-}$ granules (4.72 ± 0.05 μm × min^{-1}) (Figure 6B, left). In contrast, the displacement, meaning the distance between the first and last time points of a track, was decreased by 15% in *Myh9*$^{-/-}$ MKs (1.70 ± 0.02 μm vs 1.43 ± 0.02 μm for the WT and *Myh9*$^{-/-}$ MKs, respectively, $P < .0001$) (Figure 6B, right). These data indicate that whereas myosin deficiency does not affect organelle movement speed, it may limit the distance of organelle traveling.

Absence of myosin IIA impairs F-actin organization

Within cells, organelle transport is strongly dependent on the dynamics of microtubule and actin cytoskeletal tracks.[16] Actin filaments serve as "rails" for the myosin-based traveling of organelles,[16-18] and as a support for their location and distribution.[19-21] We therefore investigated whether the F-actin cytoskeleton was affected by the absence of myosin. Progenitor cells from bone marrow were cultured for 4 days and allowed to adhere to a fibronectin-coated surface. Actin filaments were then labeled with AF-488 phalloidin. Compared with the WT, *Myh9*$^{-/-}$ MKs exhibited strongly defective actin rearrangement following adhesion to fibronectin. The actin filaments on the basal side of the cells appeared to be shorter and stress fibers were absent. Unlike in WT MKs, where F-actin was strongly present in the cell cortex and distributed relatively evenly throughout the cytoplasm, *Myh9*$^{-/-}$ cells had little cortical F-actin. Moreover, clusters of F-actin were observed in the cytoplasm of these MKs (Figure 7A) suggesting that myosin IIA is involved in structuring the actin cytoskeleton network.

To determine whether F-actin organization was also affected in *Myh9*$^{-/-}$ MKs in situ and could explain the abnormal granule clustering, we further analyzed the F-actin cytoskeleton by confocal microscopy using AF-488 phalloidin labeling of bone marrow fragments (Figure 7B). F-actin was again abundant in the cell cortex of WT MKs, forming a belt in the peripheral zone and delineating the DMS in the cytoplasm, as previously reported.[22] In smaller immature

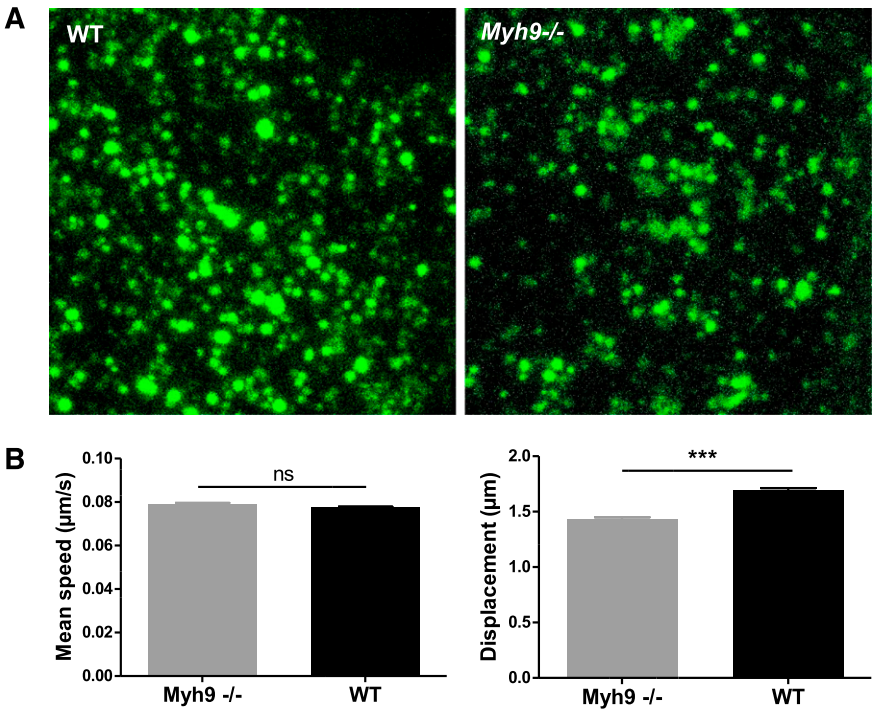

Figure 6. Impaired organelle motility in *Myh9*$^{-/-}$ MKs. (A) Cultured *Myh9*$^{-/-}$ and WT MKs were imaged using videomicroscopy after AF-488–fibrinogen incorporation. Image showing the maximal confocal projection of a MK cytoplasm portion (5.5 μm thickness). (B) Labeled organelles were tracked and their mean speed and displacement were measured. Only tracks that were longer than 25 seconds were evaluated to reliably determine the displacement. Data are mean ± SEM of 5260 (WT) and 3479 (*Myh9*$^{-/-}$) granules from at least 3 independent experiments. ***$P < .0001$. ns, not significant.

MKs, F-actin appeared to be more diffuse in the cytoplasm and did not form clusters. Conversely, no such high peripheral F-actin content was observed in *Myh9*$^{-/-}$ MKs. In addition, clusters of F-actin similar to those observed in vitro were present in the cytoplasm of the *Myh9*$^{-/-}$ cells (Figure 7B), indicating a strongly defective F-actin organization. These F-actin aggregates did not colocalize with VWF-positive granules as observed by confocal microscopy of *Myh9*$^{-/-}$ MKs in situ (not shown), suggesting that granule clusters do not result from localized tethering onto these F-actin clusters.

Actin filaments are dynamic structures constantly submitted to polymerization and depolymerization. To find out whether myosin affects actin dynamics, we measured actin polymerization in thrombin-activated platelets by flow cytometry. Actin polymerization was significantly reduced in myosin IIA–deficient platelets (43% less actin polymerization) compared with WT cells (supplemental Figure 2).

Overall, these data demonstrate the involvement of myosin IIA in actin cytoskeleton organization and dynamics and suggest that the defective F-actin network in *Myh9*$^{-/-}$ MKs affects the intracellular organelle and distribution.

Discussion

In the present study, we show that myosin IIA deficiency in the mouse or a myosin IIA mutation in a patient alters the organelle distribution pattern in platelets. The main findings are that the absence of myosin critically modifies F-actin organization within MKs and impairs organelle motility in the cytoplasm of these cells. As a result, abnormal organelle clustering in MKs directly translates into a heterogeneous organelle distribution in platelets.

On the grounds of early in situ electron microscopy visualization and more recent in vivo real-time imaging in living mice, it is now well documented that MKs shed cytoplasmic fragments exceeding the platelet size into the bone marrow sinusoids.[12,23-25] This is compatible with the model of preplatelets, assuming that these represent large MK fragments which are thought to remodel into proplatelets within the bloodstream before releasing platelets of normal size.[3,26] On the basis of this model it may be expected that the organelle delivery to platelets will depend on (1) the organelle distribution in the released MK fragments, which stems from the distribution pattern in MKs, and (2) the individual organelle traffic along microtubule tracks, during shear-induced proplatelet remodeling in the blood circulation.

We propose here that the heterogeneity of the granule distribution in *Myh9*$^{-/-}$ platelets originates from the abnormal organelle distribution already present in MKs. Indeed, organelle transport along the proplatelet shaft does not appear to be affected in *Myh9*$^{-/-}$ mice, as shown by the normal α granule content of the proplatelet buds formed by cultured MKs (Figure 3). These results are consistent with previous work[5] showing that granule translocation along the microtubules lining the proplatelet shafts is independent of actin and confirm that unlike the microtubular cytoskeleton, the actomyosin cytoskeleton is not crucial for the traffic within proplatelets. Hence, the presence of empty or crowded platelets can be explained by the heterogeneity in the organelle content already present in the large preplatelet fragments released in the sinusoid vessels. In agreement with this hypothesis, we observed in *Myh9*$^{-/-}$ bone marrow sinusoids some MK fragments with either very few or numerous organelles, which would inevitably result in low-content or high-content platelets, respectively (Figure 4A). In turn, this heterogeneity in the preplatelet content directly reflects the abnormal organelle distribution present in the cytoplasm of *Myh9*$^{-/-}$ MKs. This is summarized in Figure 4B.

The way granules are distributed in the cytoplasm during MK maturation is still unresolved. Interestingly, we observed that in immature WT MKs, maturing granules and mitochondria form clusters close to the nucleus, in proximity or juxtaposed to membrane structures such as RER or developing DMS (Figure 2B; supplemental Figure 1). Upon maturation, organelles will be homogeneously redistributed to the granular zone. These observations in immature WT MKs are reminiscent of the abnormal granule positioning observed in "mature" *Myh9*$^{-/-}$ MK/platelets (Figure 2B), suggesting

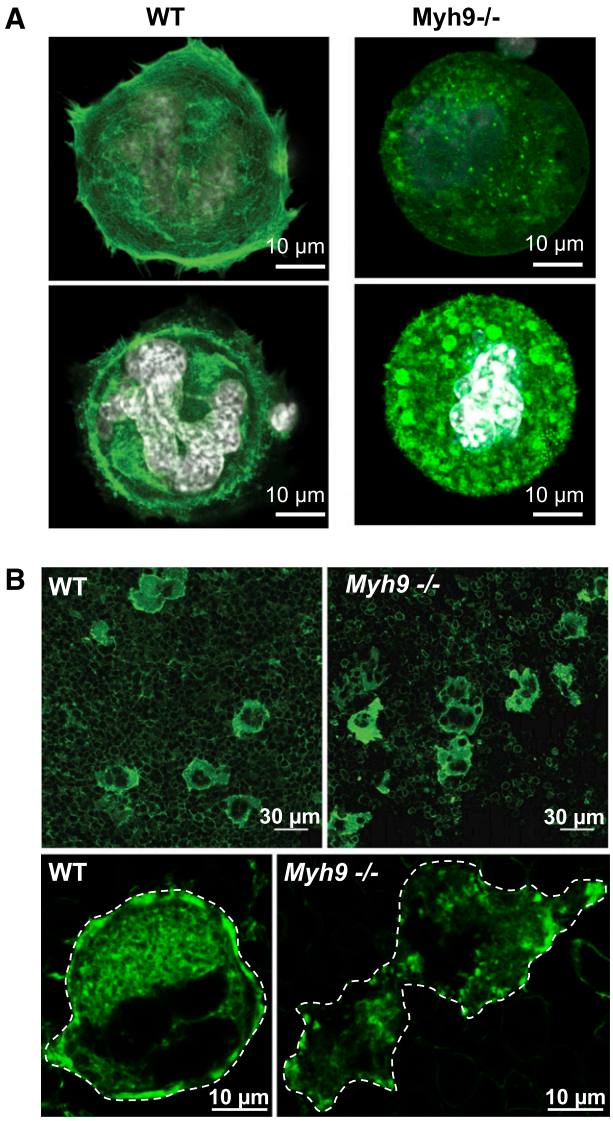

Figure 7. Defective actin organization in *Myh9*$^{-/-}$ MKs. (A) In vitro–differentiated WT and *Myh9*$^{-/-}$ MKs were allowed to adhere to fibronectin-coated coverslips for 1 hour and F-actin was visualized by AF-488 phalloidin labeling. Confocal images were taken at the base of a cell in contact with the coverslip (top panels) and in the plane of the white-labeled nucleus of the same cell (bottom panels). Images are representative of 3 independent experiments. (B) F-actin labeling of bone marrow using AF-488 phalloidin. (Top panels) Wide fields from WT and *Myh9*$^{-/-}$ marrow samples. (Bottom panels) Detail showing the F-actin distribution within a WT (left) and a *Myh9*$^{-/-}$ (right) MK. Dotted lines delineate the MKs. Images are representative of at least 3 different bone marrow samples for each genotype.

that *Myh9*$^{-/-}$ MKs granule redistribution is impaired during the maturation process. Because granules and DMS are often found in close proximity in immature WT MKs, and DMS is impaired in *Myh9*$^{-/-}$ MKs,[9] it could be that normal granule distribution within the platelet territories of mature MKs directly depends on DMS organization, or that both the DMS development and the granule distribution depend on actomyosin activity.

In this work, we show that myosin IIA is associated with the cytoplasmic face of platelet granules and mitochondria. The way in which myosin IIA binds to platelet organelles is still unknown, and it could bind as a single molecule like in lytic granules of natural killer cells[27] or as larger microfilaments. F-actin has been suggested to be present at the periphery of individual platelet organelles,[14] but our results demonstrate that the association of myosin with organelle membranes is mainly independent of F-actin. Myosin IIA could bind directly to the lipid bilayer,[28,29] or it may associate indirectly through binding to organelle-associated proteins.[30] Its constitutive association with the platelet granule surface might play a role in anchorage of the granules to F-actin network to allow positioning within the mature MK. F-actin networks indeed provide the scaffold for the anchorage and positioning of secretory granules,[20,31,32] and F-actin–disrupting agents in melanocytes have for instance been shown to result in the formation of melanosome aggregates.[33-35]

We observed here that myosin deficiency modestly but significantly impairs organelle motility within MKs, in terms of mean displacement (Figure 6). Of note, our observations of granule movements within live MKs took into account all types of displacement involving both microtubules and F-actin, which may have underestimated the real impact of myosin deficiency on F-actin–mediated transport. Because the mean speed is unchanged, myosin IIA bound to the organelle is probably not a critical motor per se for the motion of granules. This is in accordance with the view that myosin IIA, in contrast to nonconventional myosins which can exhibit processive activity, is unlikely to directly transport cargo over long distances.[31,36] By contrast, the decreased mean displacement of *Myh9*$^{-/-}$ granules, although modest, suggests modifications of cytoskeletal tracks. It was indeed previously shown that F-actin growth increases the distances traveled by organelles by increasing the effective transport track's length.[17,18,37] In accordance with this hypothesis, we observed that the spatial organization of F-actin is abnormal *in Myh9*$^{-/-}$ MKs and actin polymerization is decreased in these platelets, indicating a role of myosin IIA in F-actin dynamics in MKs. The involvement of myosin II in actin polymerization/structuration has already been documented for F-actin cross-linking[38,39] or for catalyzing actin assembly at focal adhesions[39] or in dynamic structures where rapid actin filament turnover is required.[40-42]

Thus, myosin IIA is likely to contribute to organelle distribution by organizing the actin meshwork necessary for organelle tethering and transport. This is in agreement with previous data using mouse lines deficient in ADF/cofilin in which actin turnover is impaired. In these mice, the platelets present an aberrant granule distribution similar to what is observed in *Myh9*$^{-/-}$ platelets.[43] Similarly, mice deficient in actin interacting protein-1 (AIP1), an actin-binding protein accelerating cofilin activity, display macrothrombocytopenia and an irregular distribution of granules in both platelets and MKs.[44]

In summary, our data shed new light on the mechanisms of granule distribution in platelets. We show here that myosin IIA is required for normal granule positioning during MK maturation, by mechanisms involving a role of myosin IIA in F-actin cytoskeleton structuration. Our results indicate that in addition to a proper traffic of organelles along microtubular tracks present in the proplatelets, an even distribution of organelles within platelets critically depends on prior homogeneous organelle distribution in the cytoplasm of mature MKs, which requires myosin IIA.

Acknowledgments

We thank Harry Heijnen for critical reading of the manuscript, Monique Freund for supervising the animal facilities, and Patricia Laeuffer for excellent technical assistance. We also thank Juliette N. Mulvihill for reviewing the English of the manuscript.

This work was supported by the Association de Recherche et Développement en Médecine et Santé Publique and the European

Union through the European Regional Development Fund. C.L. is the recipient of a "contrat d'interface" between the EFS and the Institut National de la Santé et de la Recherche Médicale.

Authorship

Contribution: F. Pertuy performed experiments and prepared the figures; A.E., F. Proamer, and J.-Y.R. performed electron microscopy; J.W. performed granule isolation and western blotting; C.L. and C.G. designed the study, supervised the experiments, interpreted the data, and wrote the manuscript; and F.L. interpreted the data and wrote the manuscript.

Conflict-of-interest disclosure: The authors declare no competing financial interests.

Correspondence: Catherine Léon, UMR_S949 Inserm-Université de Strasbourg, Etablissement Français du Sang-Alsace (EFS-Alsace), 10, rue Spielmann, B.P. No. 36, 67065 Strasbourg Cedex, France; e-mail: catherine.leon@efs-alsace.fr.

References

1. Zucker-Franklin D. Megakaryocytes and platelets. In: Zucker-Franklin D, Grossi CE, eds. *Atlas of Blood Cells,* Vol. 2. Milan, Italy: Edi. Ermes, 2003: 788-791.
2. Blair P, Flaumenhaft R. Platelet alpha-granules: basic biology and clinical correlates. *Blood Rev.* 2009;23(4):177-189.
3. Thon JN, Italiano JE. Platelet formation. *Semin Hematol.* 2010;47(3):220-226.
4. Italiano JE Jr, Lecine P, Shivdasani RA, Hartwig JH. Blood platelets are assembled principally at the ends of proplatelet processes produced by differentiated megakaryocytes. *J Cell Biol.* 1999; 147(6):1299-1312.
5. Richardson JL, Shivdasani RA, Boers C, Hartwig JH, Italiano JE Jr. Mechanisms of organelle transport and capture along proplatelets during platelet production. *Blood.* 2005;106(13): 4066-4075.
6. Léon C, Eckly A, Hechler B, et al. Megakaryocyte-restricted MYH9 inactivation dramatically affects hemostasis while preserving platelet aggregation and secretion. *Blood.* 2007;110(9):3183-3191.
7. Heath KE, Campos-Barros A, Toren A, et al. Nonmuscle myosin heavy chain IIA mutations define a spectrum of autosomal dominant macrothrombocytopenias: May-Hegglin anomaly and Fechtner, Sebastian, Epstein, and Alport-like syndromes. *Am J Hum Genet.* 2001;69(5): 1033-1045.
8. Cazenave JP, Ohlmann P, Cassel D, Eckly A, Hechler B, Gachet C. Preparation of washed platelet suspensions from human and rodent blood. *Methods Mol Biol.* 2004;272:13-28.
9. Eckly A, Strassel C, Freund M, et al. Abnormal megakaryocyte morphology and proplatelet formation in mice with megakaryocyte-restricted MYH9 inactivation. *Blood.* 2009;113(14): 3182-3189.
10. Strassel C, Eckly A, Léon C, et al. Hirudin and heparin enable efficient megakaryocyte differentiation of mouse bone marrow progenitors. *Exp Cell Res.* 2012;318(1):25-32.
11. Eckly A, Heijnen H, Pertuy F, et al. Biogenesis of the demarcation membrane system (DMS) in megakaryocytes [published online ahead of print October 23, 2013]. *Blood.*
12. Junt T, Schulze H, Chen Z, et al. Dynamic visualization of thrombopoiesis within bone marrow. *Science.* 2007;317(5845):1767-1770.
13. Zhang L, Orban M, Lorenz M, et al. A novel role of sphingosine 1-phosphate receptor S1pr1 in mouse thrombopoiesis. *J Exp Med.* 2012;209(12): 2165-2181.
14. Flaumenhaft R, Dilks JR, Rozenvayn N, Monahan-Earley RA, Feng D, Dvorak AM. The actin cytoskeleton differentially regulates platelet alpha-granule and dense-granule secretion. *Blood.* 2005;105(10):3879-3887.
15. Woronowicz K, Dilks JR, Rozenvayn N, et al. The platelet actin cytoskeleton associates with SNAREs and participates in alpha-granule secretion. *Biochemistry.* 2010;49(21):4533-4542.
16. Ross JL, Ali MY, Warshaw DM. Cargo transport: molecular motors navigate a complex cytoskeleton. *Curr Opin Cell Biol.* 2008;20(1): 41-47.
17. Semenova I, Burakov A, Berardone N, et al. Actin dynamics is essential for myosin-based transport of membrane organelles. *Curr Biol.* 2008;18(20): 1581-1586.
18. Zajac AL, Goldman YE, Holzbaur EL, Ostap EM. Local cytoskeletal and organelle interactions impact molecular-motor-driven early endosomal trafficking. *Curr Biol.* 2013;23(13):1173-1180.
19. Boldogh IR, Pon LA. Mitochondria on the move. *Trends Cell Biol.* 2007;17(10):502-510.
20. Hume AN, Seabra MC. Melanosomes on the move: a model to understand organelle dynamics. *Biochem Soc Trans.* 2011;39(5):1191-1196.
21. Minin AA, Kulik AV, Gyoeva FK, Li Y, Goshima G, Gelfand VI. Regulation of mitochondria distribution by RhoA and formins. *J Cell Sci.* 2006; 119(Pt 4):659-670.
22. Schulze H, Korpal M, Hurov J, et al. Characterization of the megakaryocyte demarcation membrane system and its role in thrombopoiesis. *Blood.* 2006;107(10):3868-3875.
23. Behnke O, Forer A. From megakaryocytes to platelets: platelet morphogenesis takes place in the bloodstream. *Eur J Haematol Suppl.* 1998;61: 3-23.
24. Lichtman MA, Chamberlain JK, Simon W, Santillo PA. Parasinusoidal location of megakaryocytes in marrow: a determinant of platelet release. *Am J Hematol.* 1978;4(4):303-312.
25. Penington DG, Streatfield K, Roxburgh AE. Megakaryocytes and the heterogeneity of circulating platelets. *Br J Haematol.* 1976;34(4): 639-653.
26. Thon JN, Montalvo A, Patel-Hett S, et al. Cytoskeletal mechanics of proplatelet maturation and platelet release. *J Cell Biol.* 2010;191(4): 861-874.
27. Sanborn KB, Mace EM, Rak GD, et al. Phosphorylation of the myosin IIA tailpiece regulates single myosin IIA molecule association with lytic granules to promote NK-cell cytotoxicity. *Blood.* 2011;118(22):5862-5871.
28. Li D, Miller M, Chantler PD. Association of a cellular myosin II with anionic phospholipids and the neuronal plasma membrane. *Proc Natl Acad Sci U S A.* 1994;91(3):853-857.
29. Murakami N, Elzinga M, Singh SS, Chauhan VP. Direct binding of myosin II to phospholipid vesicles via tail regions and phosphorylation of the heavy chains by protein kinase C. *J Biol Chem.* 1994;269(23):16082-16090.
30. Wu X, Sakamoto T, Zhang F, Sellers JR, Hammer JA III. In vitro reconstitution of a transport complex containing Rab27a, melanophilin and myosin Va. *FEBS Lett.* 2006;580(25):5863-5868.
31. Loubéry S, Coudrier E. Myosins in the secretory pathway: tethers or transporters? *Cell Mol Life Sci.* 2008;65(18):2790-2800.
32. Brown AC, Oddos S, Dobbie IM, et al. Remodelling of cortical actin where lytic granules dock at natural killer cell immune synapses revealed by super-resolution microscopy. *PLoS Biol.* 2011;9(9):e1001152.
33. Barral DC, Seabra MC. The melanosome as a model to study organelle motility in mammals. *Pigment Cell Res.* 2004;17(2):111-118.
34. Koyama YI, Takeuchi T. Differential effect of cytochalasin B on the aggregation of melanosomes in cultured mouse melanoma cells. *Anat Rec.* 1980;196(4):449-459.
35. Rogers SL, Gelfand VI. Myosin cooperates with microtubule motors during organelle transport in melanophores. *Curr Biol.* 1998;8(3):161-164.
36. O'Connell CB, Tyska MJ, Mooseker MS. Myosin at work: motor adaptations for a variety of cellular functions. *Biochim Biophys Acta.* 2007;1773(5): 615-630.
37. Schuh M. An actin-dependent mechanism for long-range vesicle transport. *Nat Cell Biol.* 2011; 13(12):1431-1436.
38. Shutova M, Yang C, Vasiliev JM, Svitkina T. Functions of nonmuscle myosin II in assembly of the cellular contractile system. *PLoS ONE.* 2012; 7(7):e40814.
39. Rossier OM, Gauthier N, Biais N, et al. Force generated by actomyosin contraction builds bridges between adhesive contacts. *EMBO J.* 2010;29(6):1055-1068.
40. Giannone G, Dubin-Thaler BJ, Rossier O, et al. Lamellipodial actin mechanically links myosin activity with adhesion-site formation. *Cell.* 2007; 128(3):561-575.
41. Medeiros NA, Burnette DT, Forscher P. Myosin II functions in actin-bundle turnover in neuronal growth cones. *Nat Cell Biol.* 2006;8(3):215-226.
42. Rex CS, Gavin CF, Rubio MD, et al. Myosin IIb regulates actin dynamics during synaptic plasticity and memory formation. *Neuron.* 2010;67(4): 603-617.
43. Bender M, Eckly A, Hartwig JH, et al. ADF/n-cofilin-dependent actin turnover determines platelet formation and sizing. *Blood.* 2010; 116(10):1767-1775.
44. Kile BT, Panopoulos AD, Stirzaker RA, et al. Mutations in the cofilin partner Aip1/Wdr1 cause autoinflammatory disease and macrothrombocytopenia. *Blood.* 2007;110(7): 2371-2380.